The Journal of Experimental Biology 206, 269-279

doi:10.1242/jeb.00079

Escape from viscosity: the kinematics and hydrodynamics of copepod foraging and escape swimming

Luca A. van Duren* and John J. Videler

Department of Marine Biology, University of Groningen, PO Box 14, 9750 AA Haren, the Netherlands

*Author for correspondence at present address: NIOO-CEME/KNAW, PO Box 140, 4400 AC Yerseke, the Netherlands

Accepted 14 October 2002

Summary

Feeding and escape swimming in adult females of the calanoid copepod *Temora longicornis* Müller were investigated and compared. Swimming velocities were calculated using a 3-D filming setup. Foraging velocities ranged between 2 and 6 mm s^{-1}, while maximum velocities of up to 80 mm s^{-1} were reached during escape responses. Foraging took place at Reynolds numbers between 2 and 6, indicating that viscous forces are considerable during this swimming mode. Inertial forces are much more important during escape responses, when Reynolds numbers of more than 100 are reached.

High-speed film recordings at 500 frames s^{-1} of the motion pattern of the feeding appendages and the escape movement of the swimming legs revealed that the two swimming modes are essentially very different. While foraging, the first three mouth appendages (antennae, mandibular palps and maxillules) create a backwards motion of water with a metachronal beating pattern. During escape movements the mouth appendages stop moving and the swimming legs beat in a very fast metachronal rhythm, accelerating a jet of water backwards. The large antennules are folded backwards, resulting in a streamlined body shape.

Particle image velocimetry analysis of the flow around foraging and escaping copepods revealed that during foraging an asymmetrical vortex system is created on the ventral side of the animal. The feeding motion is steady over a long period of time. The rate of energy dissipation due to viscous friction relates directly to the energetic cost of the feeding current. During escape responses a vortex ring appears behind the animal, which dissipates over time. Several seconds after cessation of swimming leg movements, energy dissipation can still be measured. During escape responses the rate of energy dissipation due to viscous friction increases by up to two orders of magnitude compared to the rate when foraging.

Key words: copepod, *Temora longicornis*, swimming, hydrodynamics, kinematics, escape response, feeding current, Reynolds number regime.

Introduction

Most aquatic animals are designed to operate either at low, or at high Reynolds numbers. Pelagic copepods are a notable exception. Many calanoid copepods exhibit different types of swimming behaviour, for which they use different groups of swimming appendages. Routine swimming with the feeding appendages is predominantly governed by viscous forces (Strickler, 1975; Alcaraz et al., 1980; Koehl and Strickler, 1981). Calanoid copepods generally use the swimming legs for rapid movements of short duration, such as escape responses, hops or, in the case of predatory copepods, forward lunges to grasp prey (Jonsson and Tiselius, 1990; Tiselius and Jonsson, 1990; Hwang et al., 1994; Yen and Strickler, 1996). During escape responses, some copepods can reach velocities of up to 200 body lengths s^{-1}, corresponding to Reynolds numbers of around 500 (Strickler, 1975).

Temora longicornis Müller is one of the most abundant copepods in the temperate coastal waters of the Northern hemisphere. It spends around 99% of its time slowly cruising or hanging nearly stationary while the feeding appendages are moving (Tiselius and Jonsson, 1990; van Duren and Videler, 1995). We will refer to this type of behaviour as 'foraging'. Velocities during this swimming mode of female *T. longicornis* up to 1 mm long typically range between 2 and 6 mm s^{-1} (van Duren and Videler, 1995, 1996). *T. longicornis* is also capable of high velocity escape movements generated by the swimming legs (Singarajah, 1975; Buskey et al., 1987; van Duren and Videler, 1996). Velocities during this type of swimming have not been accurately measured.

This study aims to investigate the swimming velocities, motion patterns, appendage kinematics and flow characteristics associated with foraging and escaping in *T. longicornis* and to estimate the energetic cost of both types of swimming behaviour.

Materials and methods

Animals

Temora longicornis Müller were cultured in the laboratory

under conditions similar to those described by Klein Breteler and Gonzales (1986). The animals were kept on a diet of small flagellate algae (*Rhodomonas* sp. and *Isochrysis galbana*) from continuous cultures. The heterotrophic flagellate *Oxyrrhis marina* was also present in the culture tanks and was the main food source for the larger copepod stages. The temperature of the culture was maintained at 15°C. In all the different experiments only apparently healthy, undamaged adult females were used. The females were selected under a dissecting microscope with a cold light source, under climate controlled conditions to avoid temperature shocks.

Swimming velocity measurements

The foraging and escape speeds of the copepods were measured in a 3-D filming setup (van Duren and Videler, 1995). Through a set of mirrors two orthogonal views of an aquarium (dimensions 10 cm×10 cm×12 cm) were projected into the lens of a video camera (I2S). The camera was connected to a Sony U-matic video recorder, running at 25 frames s^{-1}. Illumination was provided by two high-output infra-red light-emitting diodes. Each light-emitting diode was placed in the focus of a lens (diameter 10 cm) behind the aquarium, creating a parallel light beam, which is projected through the aquarium straight into the lens of the camera. This yields silhouette images with the animals showing as black dots against a white background.

The resulting tapes were analysed using a computer image analysis system, which allowed processing of individual fields of video frames, resulting in a maximum temporal resolution of 50 data points s^{-1}. *X*, *Y* and *Z* coordinates of the position of the animals in each frame were used to calculate instantaneous swimming speeds (van Duren and Videler, 1995).

Prior to the experiments groups of 10 adult females were selected and left in the experimental setup to acclimatise for approximately 15 min.

A 2 s light pulse of 230 μE m^{-2} s^{-1} (measured on top of the aquarium) provided by a spotlight (150 W, Philips) mounted above the setup was used to provoke escape reactions without causing any disturbances in the water. The temperature during the experiments was maintained at 15°C.

High-speed film kinematic analysis

A Locam 16 mm high-speed camera (Redlake, model 51) capable of recording up to 500 frames s^{-1} was mounted on top of a dissecting microscope. Adult females were tethered to a very thinly drawn glass pipette using a suction restraint technique (Gill, 1987; van Duren et al., 1998). The pipette was mounted on a micromanipulator, which in turn was mounted on the base of the microscope. The females were placed with their lateral side to the camera, and their body axis horizontal with respect to the camera. Recordings were made at 300 and at 500 frames s^{-1} of the swimming movements of the feeding appendages, and the escape swimming with the pereopods. Escape responses were evoked by a gentle tap on the base of the micromanipulator holding the pipette with the animal. The size of the container used for filming was 6×6×4 cm.

The films were subsequently projected on a Vanguard Motion Analyser. Each frame was digitized by recording the projected image with a video camera, connected directly to an image analysis system. The coordinates of the tip position of each appendage involved in the feeding movement: antenna (A2), mandibular palp (Mdb), maxillule (mx1) maxilla (mx2) and maxillipede (mxp), and in the escape response: pereopods 1–4 (p1, p2 etc), were digitised manually.

Particle image velocimetry analysis

A detailed description of the filming set-up and the general experimental procedure for particle image velocimetry (PIV) experiments can be found in the accompanying paper (van Duren et al., 2003). Tethered female copepods were positioned in the light sheet, with their lateral side towards the camera. The light sheet was positioned through the centre of the copepod along the rostral-caudal axis, perpendicular to the antennules. Particle movement around the feeding and escaping animals was recorded with a video camera (I2S) operating at 25 frames s^{-1}, fitted with a 35 mm macro lens and a 30 mm extension ring. Shutter speed was set at 1/125 s. The resulting image covered a field of view of 8.1 mm×5.9 mm. The camera was connected to a Sony U-Matic video recorder.

The choice of the temporal resolution was based on the flow velocities. During and immediately after swimming leg movement a 0.02 s time interval was taken, but around the foraging animal and more than 0.2 s after swimming leg movement had ceased, a 0.04 s time step was taken, to ensure sufficient particle displacement between the two images.

Flow fields were calculated from the particle displacements measured in the subsequent images (Stamhuis and Videler, 1995). These flow fields were expressed in fields of regularly spaced velocity vectors. The resolution of the flow field (i.e. the size of the grid cells) was chosen on the basis of the sub-image size of the sub-image PIV analysis. For the flow fields of these experiments each grid cell represents a surface area of 0.048 mm^2.

Gradient parameters such as vorticity, shear and spatial acceleration rates were calculated for each cell from the partial derivatives of the *x* and *y* components of the velocity vectors (**u** and **v**) (Stamhuis and Videler, 1995; van Duren et al., 2003).

Post-processing

The volume of influence around a copepod was defined as the volume of water around the animal where the shear rate was more than 0.7 s^{-1} (van Duren et al., 1998).

By its nature, laser sheet PIV yields two-dimensional results. However, carefully positioning the animal so that the main direction of flow is parallel to the laser sheet ensures that the amount of out-of-plane motion is minimal and the error incurred by ignoring the contribution of this component is assumed to be very small. Flow around copepods is known to be symmetrical when viewed dorsally, but when viewed laterally there are significant differences between the dorsal and the ventral flows (Fields and Yen, 1993; van Duren et al., 2003). Our images show the lateral view. To estimate the

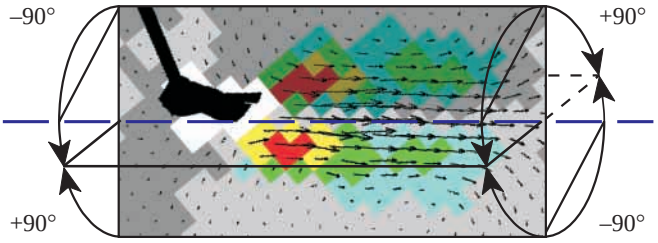

Fig. 1. Construction of the 3-D flow field by rotating the particle image velocimetry flow field around a central axis.

volume of influence, we rotated the velocity vectors around an imaginary axis similar to that described in van Duren et al. (1998).

When a vortex ring was present behind the animal, we calculated a line straight through the centre of this vortex. Although the vortex rings were not always symmetrical, the line where the sign of vorticity changed was always a straight one, parallel to the direction of the jet (Fig. 1). This line was taken to be the centre of the vortex. When no vortex ring was present (e.g. when the animal was foraging), the rotation axis was assumed to run through the feeding appendages of the animal, parallel to the body axis.

To estimate the volume of influence (V_{tot}), the flow field was rotated over +90° and –90°, around the calculated axis. In other words, we assume the part of the flow field above the rotation axis to be representative of the flow dorsal to the animal and the part below this axis to represent the flow ventral to the animal. The total volume of influence (V_{tot}) is the sum of the volumes of two half cylinders, one above and one below the plane through the rotation axis (Fig. 1):

$$V_{tot} = V_i + V_j , \quad (1)$$

where

$$V_i = \sum(\pi \times A_i \times r_i) \quad (2)$$

and

$$V_j = \sum(\pi \times A_j \times r_j) . \quad (3)$$

A is the surface area of a cell with a shear rate >0.7 s^{-1}, r is the distance of the centre of this cell to the rotation axis and indices i and j refer to cells above and below the rotation axis, respectively.

Viscous energy dissipation

Within the volume of influence the rate of energy dissipation through viscous friction (P) can be estimated as:

$$P = \nu\sum V_i\Phi_i + \mu\sum V_j\Phi j , \quad (4)$$

where P is expressed in W, ν is the dynamic viscosity (kg m^{-1} s^{-1}) and volume elements V_i and V_j (m^3) as defined above. The dissipation function Φ is expressed in s^{-2} (Yen et al., 1991; van Duren et al., 1998):

$$\Phi_{XY} = \left(\frac{\partial \mathbf{u}}{\partial x}\right)^2 + \left(\frac{\partial \mathbf{v}}{\partial y}\right)^2 + \left(\frac{\partial \mathbf{u}}{\partial y} + \frac{\partial \mathbf{v}}{\partial x}\right)^2 . \quad (5)$$

During foraging the flow field stays stable over a long period of time. Therefore, the amount of energy the animal puts into the water is balanced by the amount of energy dissipating due to viscous friction. The rate of energy dissipation, calculated by the method described above, is therefore directly proportional to the power delivered by the feeding appendages. During an escape response, a vortex ring is formed. Such vortex rings contain kinetic energy, which eventually also dissipates into viscosity. By calculating the viscous energy dissipation rate in a time series of flow fields, from the start of an escape response until all the effects of the escape movement in the water have dissipated, we can calculate the total amount of energy delivered by the swimming legs. The power delivered by these appendages can be calculated by dividing the total energy loss by the amount of time the swimming legs have been moving.

In some of the flow fields the volume of influence may have been slightly underestimated due to the fact that the area where the shear rate exceeded the threshold level reached further than the field of view. However, the effect on the estimated rate of energy dissipation will have been minimal, since this is largely determined by the peak values in velocity gradients, which do not occur in the periphery of the volume of influence, but were always well within the field of view.

Results

Swimming velocity measurements

Fig. 2A shows a time–velocity record of a foraging adult female. The movement is smooth without stops or jumps and the average speed is 3.4 mm s^{-1}, well within the range of typical foraging velocities of adult females. These speeds translate into Reynolds numbers between 2 and 6, for animals with a body length of 1.2 mm (body length is here considered

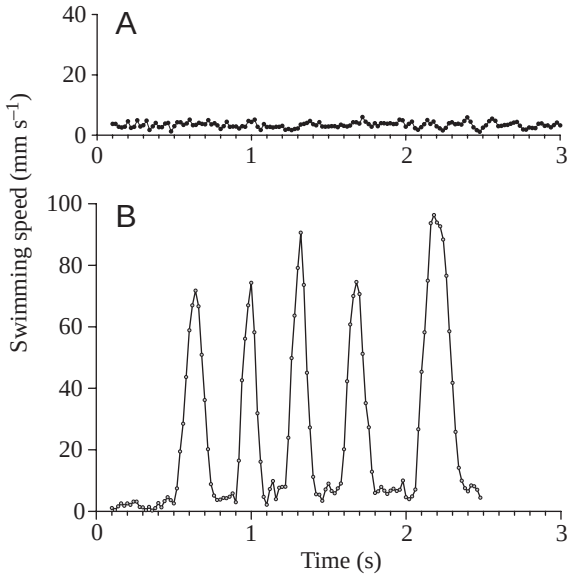

Fig. 2. (A) Swimming speed record of a foraging female *T. longicornis*. (B) Swimming speed record of an escape response of an adult female.

to be cephalothorax and urosome without the setae on the furca). Fig. 2B shows a similar record of a sequence of five escape responses of an adult female. Maximum velocities during escape movements ranged between 25.3 and 107.9 mm s^{-1}, with an average of 75.5 mm s^{-1} (N=17). Multiple jumps following a single stimulus are very common. These escape velocities correspond to Reynolds numbers between 26 and 110.

High-speed film measurements

Fig. 3A shows a record of the X-position of the tips of the five feeding appendages. The symbols in the graph correspond to the relevant appendages in the drawing of the copepod above the graph. During feeding the two large antennules are kept extended and they do not participate in any feeding or swimming movement. The feeding appendages can be divided into two groups: the antennae, the mandibular palps and the maxillules, which create the actual feeding current, and the maxillae and the maxillipeds, which appear to have the function of filtering and/or grasping particles from the feeding current. The three anterior appendages beat in an adlocomotory metachronal wave with a phase angle of 65°, with the power stroke directed backwards. The maxillule reaches its extreme anterior position before the other two appendages. While the mandibular palp and the antenna continue their recovery stroke, the maxillule starts its power stroke. When the maxillule is about halfway between its extreme positions in the power stroke, the mandibular palp starts its power stroke, while the antenna continues to complete its recovery stroke. When the maxillule has reached its extreme position and starts its recovery stroke, the antenna starts its power stroke. When the mandibular palp reaches its maximum position, its meets the forward moving maxillule and these appendages continue their recovery stroke together. They ‘meet’ with the antenna, when it reaches its extreme position. The three appendages continue their recovery stroke together for about 2 ms, until the maxillule has reached its extreme anterior position and the cycle starts again. Meanwhile, the maxilla and the maxillipede move synchronously, the maxillipede with a much larger amplitude due to its greater length. The maxillipede generally does not interfere with the movement of any of the other appendages. The tip of the maxilla meets the tip of the maxillule when the maxillule reaches its extreme posterior position. The setae of these two appendages overlap and a small volume of water is enclosed between the body of the copepod and the setae of the maxillule and maxilla. When the two appendages separate the setae probably comb each other, although this was not properly visible on the films. The maxilla and the maxillipede appear to be beating in opposite phase with the mandibular palps. The setae on these two appendages are orientated in the direction opposite to the setae on the first three appendages, and their power stroke runs from posterior to

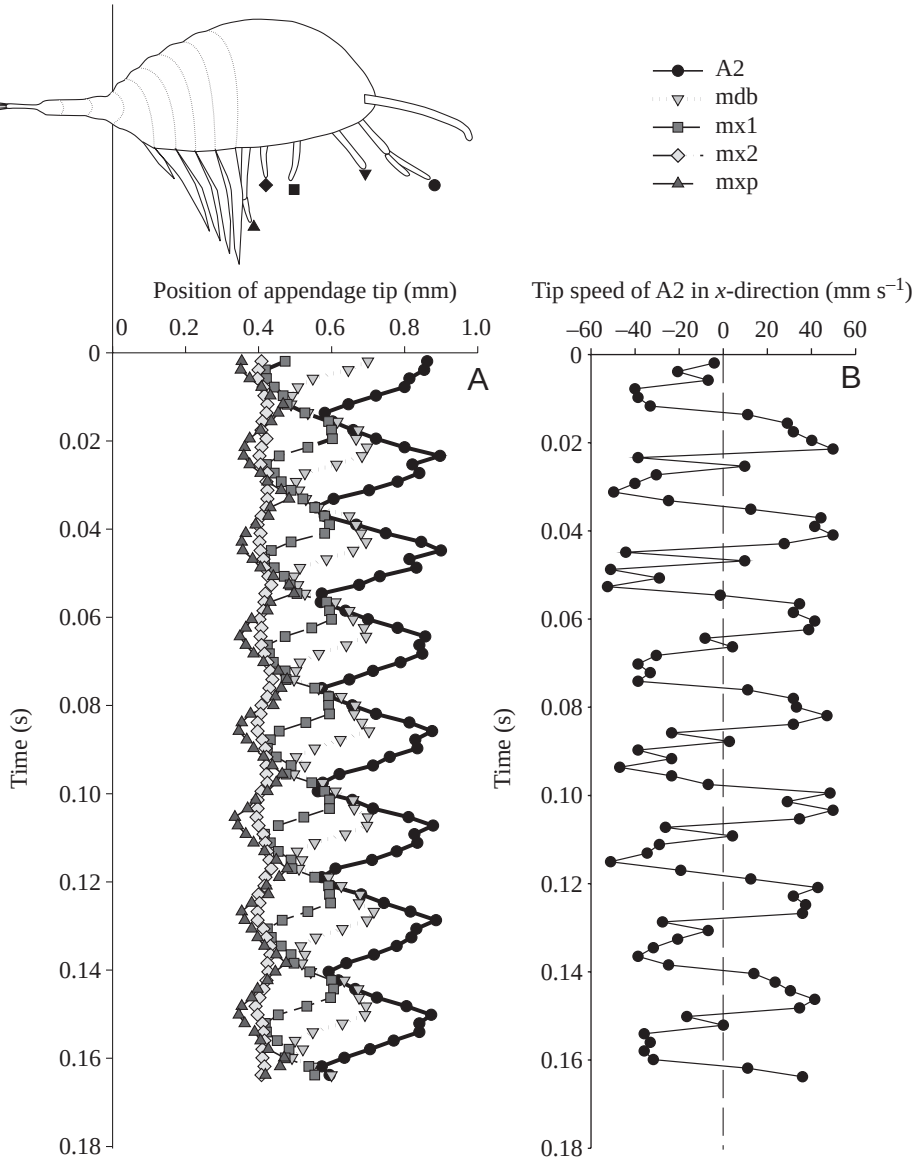

Fig. 3. (A) Tracing of the tip position of the feeding appendages of a foraging female *T. longicornis*. (B) Record of the horizontal (i.e. along the body axis) velocity component of the antenna during feeding. Note that positive values indicate the velocity during the power stroke and negative values are velocities in the opposite direction (recovery stroke).

anterior. Therefore, in terms of power and recovery stroke they are beating in phase with the mandibular palps.

The whole cycle of movement takes approximately 0.025 s, and the average beat frequency measured in the six analysed sequences of film was 40.7±8.0 Hz. Fig. 3B shows the tip speed velocity of the antenna. The average maximum tip speed of the largest feeding appendage was 43 mm s^{-1}, in both directions.

At the start of an escape response, the copepods fling the laterally extended antennules backwards and hold them close to the body during the whole time that the swimming legs are moving. No movement of the feeding appendages is visible during an escape response. These extremities do not restart moving until the swimming legs have ceased all movement and have resumed their 'foraging' position. Fig. 4A shows a record of the position of the tips of the swimming legs, p1 being the most anterior pereopod and p5 the reduced fifth swimming leg. The position of the tip of the relevant appendages corresponds with the copepod drawing above this graph. This last pair of legs was not clearly visible in all the analysed sequences, but due to its reduced size it probably does not contribute significantly to the total thrust produced.

The swimming legs are co-ordinated differently from the feeding appendages. The appendages move metachronally only during the power stroke, when the appendages beat in an adlocomotor sequence. The recovery stroke is synchronised. Of the four normal sized swimming legs, p4 is the first to start the power stroke, when it has completed its power stroke and has reached its extreme posterior position, p3 starts and completes its power stroke, then p2 and finally p1. When p1 has reached its extreme position, all four swimming legs start the combined recovery stroke, which is much slower than the individual power strokes. Fig. 4B shows a record of the tip velocity in horizontal direction of p1 (note that negative velocities represent the power stroke, i.e. a backwards movement relative to the copepod). During escape responses we measured beat frequencies of the swimming legs between 44 and 117 Hz.

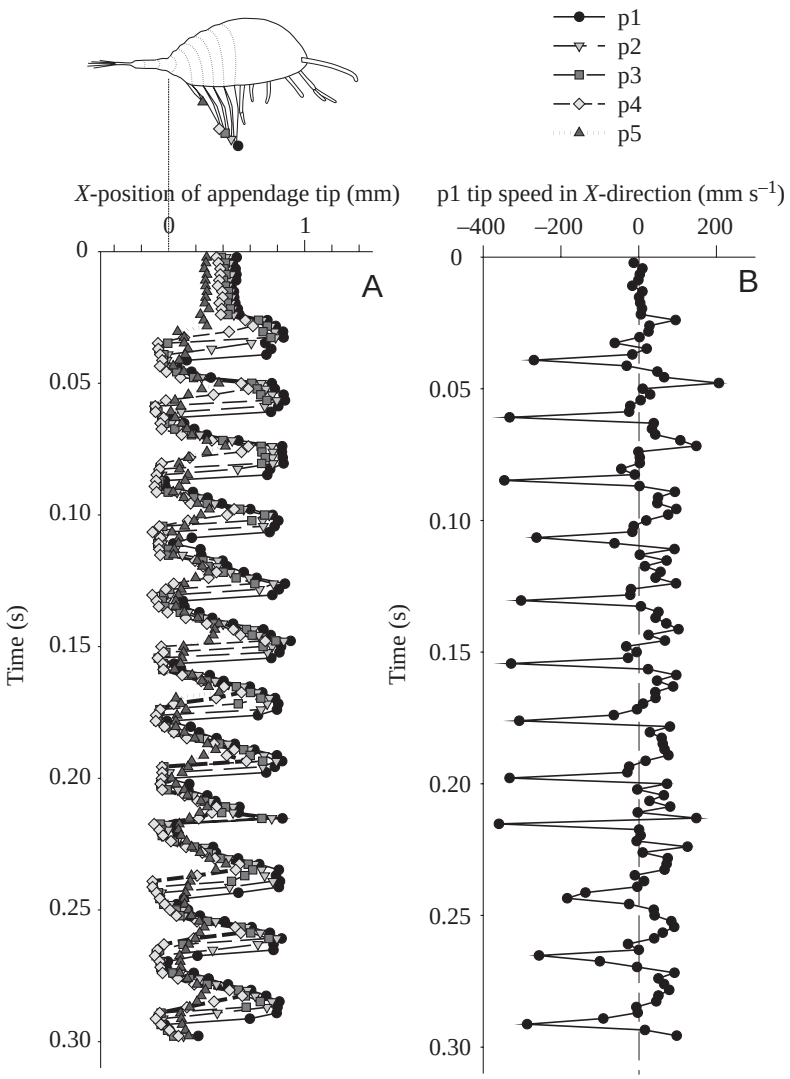

Fig. 4. (A) Tracing of the tip position of the swimming legs of an escaping female *T. longicornis*. (B) Record of the horizontal (i.e. along the body axis) velocity component of the first pair of swimming legs. Note that positive values indicate the velocity during the power stroke and negative values are velocities in the opposite direction (recovery stroke).

PIV measurements

Fig. 5A shows a flow field around a foraging adult female *T. longicornis*. Highest velocities are found around the feeding appendages, and in this area the largest velocity gradients are also found. To the ventral side of the animal is an area of relatively high vorticity (Fig. 5B); the centre of this vortex system is located just ventral from the position of the maxillipeds. The flow field does not change over time, while the animal is foraging.

During an escape response, the flow field around the animal changes markedly over time. Figs 6A–D show a sequence of flow fields of a single escape response. Fig. 6A shows the velocity distribution immediately after the start of swimming leg movement (t=0). Fig. 6B shows a similar plot at t=0.08, Fig. 6C at t=0.28 just after cessation of swimming leg movement and Fig. 6D at 0.5 s after the start of swimming leg movement.

A jet of water starts to develop as soon as the swimming legs start moving. This jet is in the centre of a vortex ring, which is however not clearly shown by the velocity plot. Fig. 7A–D shows the vorticity distribution at the same points in time as the velocity fields. After cessation of leg movement, the vortex ring moves backwards, becomes wide and dissipates altogether within 0.5–1 s.

In multiple escape responses, the next jump starts before the effects of the previous one are fully dissipated. Fig. 8A,B

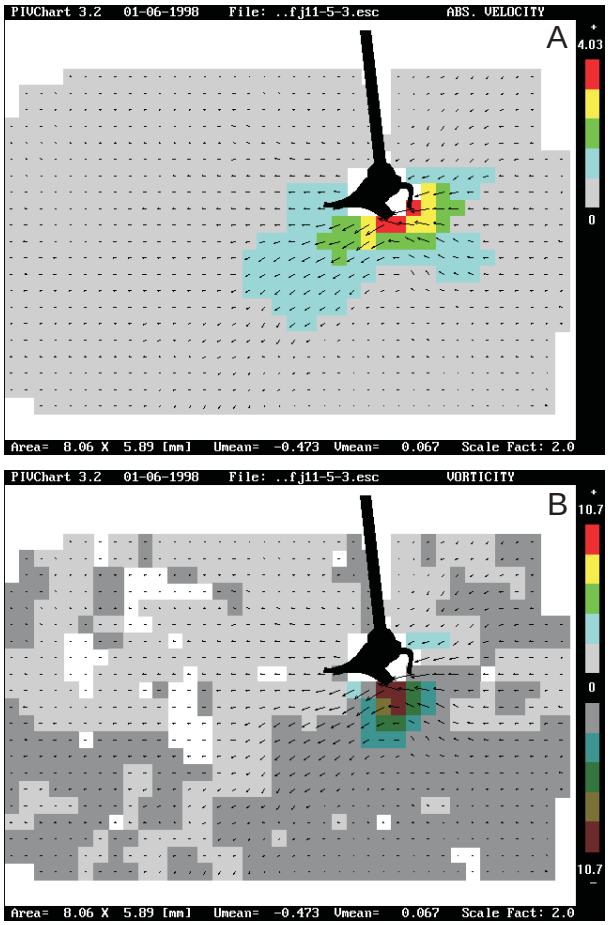

Fig. 5. (A) Velocity distribution around a foraging copepod. (B) Vorticity plot of the flow field around a foraging copepod.

shows the velocity magnitude and the vorticity distribution 0.04 s after the start of the third jump, 0.08 s after cessation of swimming leg movement of the previous jump.

The volume of influence, where the animal has a significant influence on the water movement, remains constant at approximately 10 mm^3 in foraging animals. During escape responses this changes dramatically over time. Fig. 9A–C shows the change of volume of influence over time in the three escape responses analysed here. The open symbols indicate the points in time where the swimming appendages were moving. In each graph t=0 indicates the time of the first start of swimming leg movement. The maximum volumes reached during escape responses range between 100 and 300 mm^3. A copepod of this species, with a metasome length of 0.8 mm, has a volume of approximately 0.06 mm^3, so this range corresponds to a volume of 1700–5000 times its body volume.

The total amount of energy dissipating due to viscous friction in the feeding current of an adult female *T. longicornis* is approximately 2×10^{-11} W. This value increases by 2 to 3 orders of magnitude during an escape response. Fig. 10A–C shows the viscous energy dissipation over time for all three animals. Table 1 shows for each animal the total amount of time the swimming legs have been moving, the total amount of energy dissipated into the water over the amount of time the effects of the escape response were visible and the power delivered by the swimming legs. Since in foraging females the power dissipation remains constant over time, the rate of energy dissipation in the water is balanced by the power input of the moving limbs.

Table 1. *Average power delivered by swimming appendages*

Animal	Energy (J)	Time of leg movement (s)	Mean power (W)	Power when foraging (W)
fj11	6.80×10^{-10}	0.28	2.43×10^{-9}	1.14×10^{-11}
fm11	5.52×10^{-10}	0.28	1.97×10^{-9}	3.29×10^{-11}
fe11	5.56×10^{-9}	0.60	9.26×10^{-9}	2.21×10^{-11}
Mean	2.26×10^{-9}		4.55×10^{-9}	2.21×10^{-11}

Discussion

Swimming velocities and the Reynolds number regime

T. longicornis is a relatively small copepod and although it may reach velocities equalling more than 100 body lengths s^{-1} during escape responses, it does not reach Reynolds numbers of much over 100. Strickler (1975) reported escape velocities for *Cyclops scutifer* of up to 500 mm s^{-1}, corresponding to a Reynolds number of about 500. *Euchaeta rimana*, a large predatory copepod, can reach swimming velocities of up to 1000 mm s^{-1}, corresponding to Reynolds numbers of approximately 2000 (Yen and Strickler, 1996), and one of the highest velocities reported for escaping calanoid copepods is measured by Pavlova (1981) for the relatively large copepod *Rhincalanus nasutus* from the Indian ocean. This species reached an amazing 2085 mm s^{-1}, corresponding to a Reynolds number of nearly 9000, a flow regime where the influences of viscous forces are minimal. These last two rather extreme examples are from large oceanic species. Although the escape abilities of *T. longicornis* appear to be modest in comparison to these larger species, they are likely to be quite comparable to those of similar sized calanoids. This high-speed escape ability appears to give copepods a significant advance in terms of predation risk over non-evasive species (Trager et al., 1994).

Limb beat patterns

In both swimming modes propulsion is generated by the metachronal beating of a group of appendages. Among invertebrates various metachronal rhythms are widely used (Sleigh and Barlow, 1980). According to these authors, metachronal patterns have two major functions. Firstly, they ensure that each individual limb can execute its motion pattern without conflict with neighbouring limbs, and secondly, one single limb, working as a member of a metachronal system, can move water more efficiently than an isolated limb. This is supported by the work of Jiang et al. (1999); in a model they varied the distribution of the same amount of total force that a copepod exerts on the water, and found that by distributing the

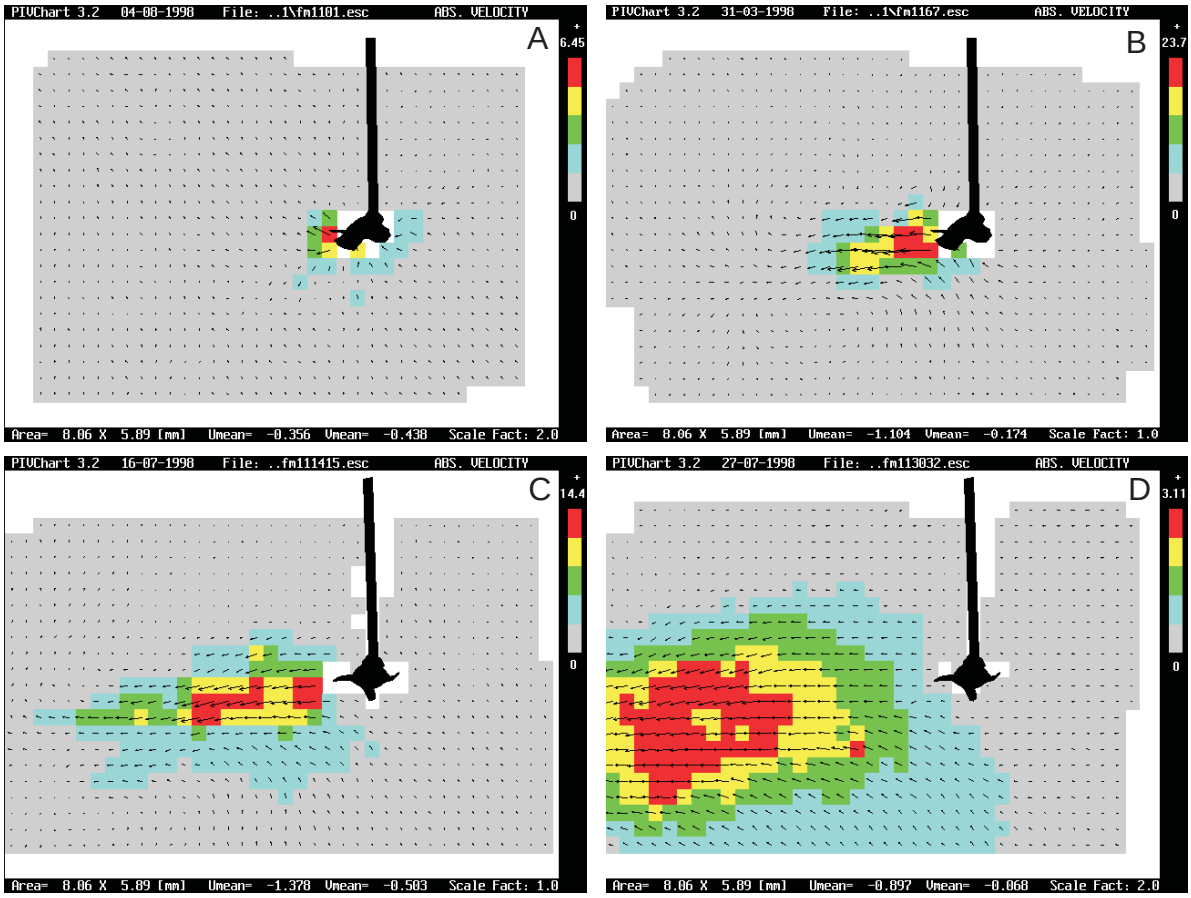

Fig. 6. Sequence of velocity distribution plots around an escaping copepod. (A) t=0 s, (B) t=0.08 s, (C) t=0.28 s and (D) t=0.5 s. Note that colour coding is a relative scale, i.e. different for each individual flow field.

force over a larger volume of water, more water was entrained over the feeding appendages at lower energetic cost.

The metachronal beat pattern of the A2, mdp and mx1 results in a slow smooth gliding motion, associated with a steady, predictable flow field. Most crustaceans that have a smooth locomotion pattern achieve this by an adlocomotory limb beat pattern, with a phase shift between the (pairs of) legs proportional to the beat cycle divided by the number of limbs (Barlow and Sleigh, 1980; Stamhuis and Videler, 1998). An increase in beat frequency often coincides with a decrease in phase angle (Sleigh and Barlow, 1980). *T. longicornis* has five pairs of feeding appendages. Based on this total number of limbs a phase shift of 60° could be expected, which is close to our measurements of 65°. However, this phase shift only applied to the three anterior appendages, the ones that are responsible for the actual propulsive motion. On the basis of three locomotive appendages, we would expect to find a phase angle of 120°, which is considerably larger than what we found. It is likely that the swimming motion of *T. longicornis* appears to be smooth, despite the small phase angle between the propulsive limbs, due to the high beat frequency of these limbs. However, it is possible that the 'recovery strokes' of the maxilla and the maxillipede also contribute to the smoothing of the swimming motion.

In contrast, the beat pattern of the swimming legs is only metachronal during the power stroke of the limbs. The successive power strokes are followed by a synchronous recovery stroke. This system maximises thrust, while the synchronous recovery stroke reduces the drag of the five pairs of appendages to little more than the amount of drag that a single pair of legs would experience during a metachronal recovery stroke (Morris et al., 1985). The resulting swimming motion and the associated flow fields are less steady than the motion produced by the fully metachronal pattern of the feeding appendages. Some copepods can maintain very high, steady escape speeds for a certain length of time due to the very high frequency of the swimming legs (Yen and Strickler, 1996). Those copepods, such as *Cyclops scutifer*, which use the swimming legs for routine swimming show a characteristic 'hop and sink' motion (Strickler, 1975).

The difference in locomotory pattern between the two groups of appendages indicates a difference in nervous locomotor control (Sleigh and Barlow, 1980) between the sets of appendages.

The metachronal movement of the swimming legs of *T. longicornis* is very similar to that of other copepods (Strickler, 1975; Alcaraz and Strickler, 1988; Morris et al., 1990). Morris et al. (1990) analysed and modelled the swimming movements

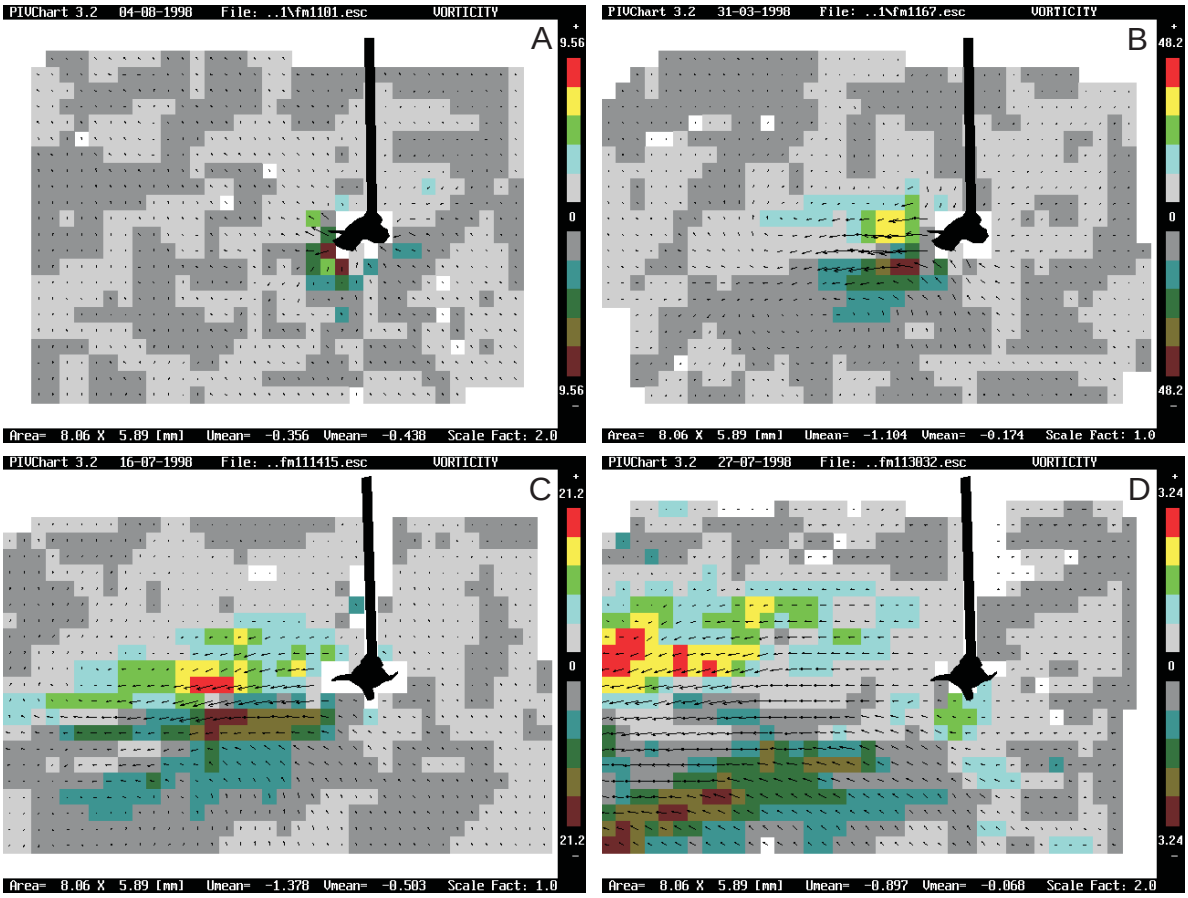

Fig. 7. Same sequence as in Fig. 6, showing vorticity plots. Note that colour coding is a relative scale, i.e. different for each individual flow field.

of *Acanthocyclops minutus*, a copepod only slightly smaller than *T. longicornis*, which swims with jumps, created using its swimming legs, similar to the escape movement of *T. longicornis*. They tested the effect of different parameters on their model predictions. Increasing the viscosity of the fluid medium decreases the jump distance, while increasing the density of the medium had the opposite effect; i.e. the higher the Reynolds regime, the more effective this propulsion system.

Flow characteristics

The conclusion that the two systems are designed to operate under different flow regimes is matched by the observed flow phenomena in the water. The flow field around a foraging *T. longicornis* is purely laminar. The flow field is also stable over a period of time and the rates of laminar shear in the feeding current are generally higher than the shear rate due to turbulence in its environment (Saiz and Kiørboe, 1995; van Duren et al., 2003). The stability and predictability of its hydrodynamical surroundings allow the copepod to use chemo- and mechanoreception to gain information about the nature, size, quality and distance of objects and organisms in its vicinity (Andrews, 1983; Légier-Visser et al., 1986; Granata and Dickey, 1991; Yen and Strickler, 1996).

The wake of an escaping copepod reaches much further. Our experiments indicate that the volume of influence increases 100- to 300-fold and a distinct vortex ring appears behind the swimming legs, similar in shape but larger in magnitude and intensity than the vortex ring reported by van Duren et al. (1998) behind a hopping copepod. The feeding current also contains an area of higher vorticity close to the feeding appendages, but no vortex rings occur. Vortex rings are strictly associated with higher Reynolds number regimes (Vogel, 1981).

In examining the flow phenomena around swimming copepods with the techniques described above, we have to take into account that the animals were tethered in order to keep them and their wake in view and in focus. When an animal is tethered, instead of moving its body through water, it moves water past its body. Although tethering does not affect the behaviour or the appendage movement of a copepod (Hwang et al., 1993), it can increase the volume of influence of an animal (Emlet, 1990). For foraging copepods in this study, as well as for the hopping copepod described in van Duren et al. (1998), the effects were probably fairly minimal. Copepods create a feeding current to draw a large volume of water over their feeding appendages, and in fact use their body drag and negative buoyancy as a ‘natural tether’ (Strickler, 1982).

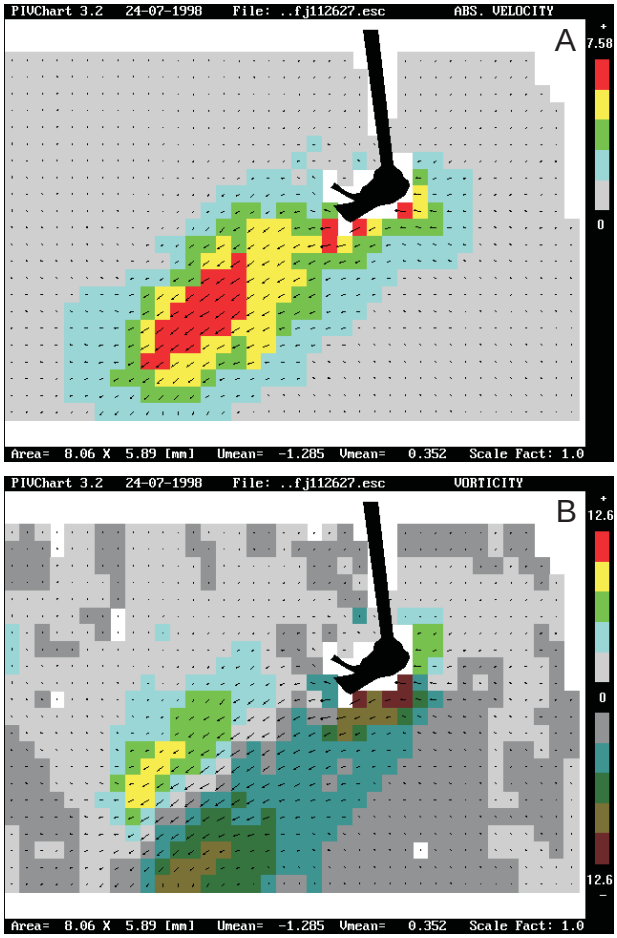

Fig. 8. Effect of multiple escape responses in the flow field. (A) Velocity distribution and (B) vorticity distribution 0.04 s after the start of a new escape response, which started 0.08 s after swimming leg movement of the previous jump ceased.

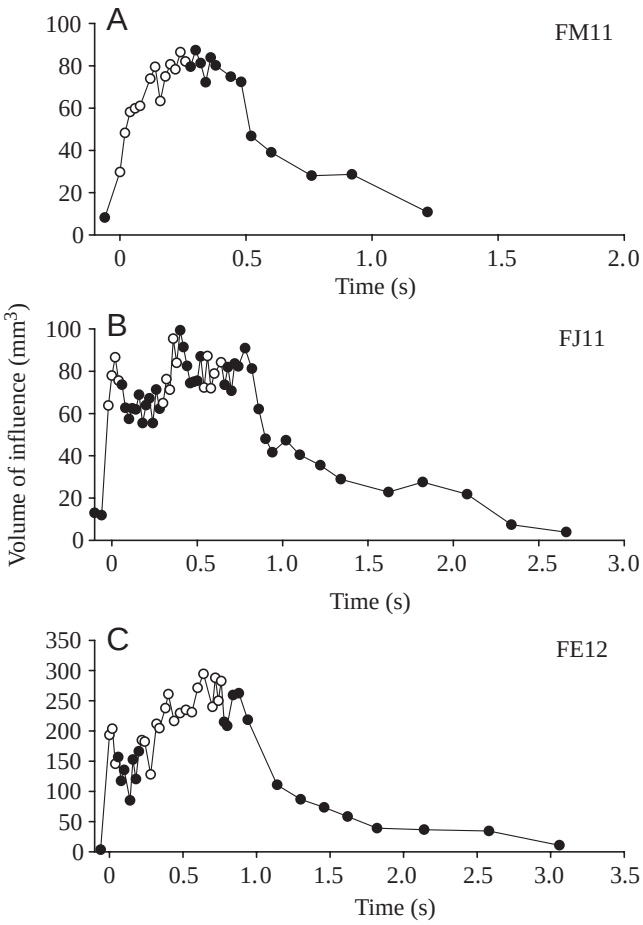

Fig. 9. (A–C). Change of volume of influence over time in escape responses of three adult female *T. longicornis*. Open symbols indicate times when the swimming appendages were moving.

Similarly, the hops described by van Duren et al. (1998) are probably created to give a hydromechanical signal. This movement is designed to shift a bulk of water, without displacing the animal very much. Escape responses, on the contrary, are designed to move an animal as fast and as far as possible away from danger, and in this case we cannot ignore the effects of the tether on the flow morphology and on the volume of influence. Yen and Strickler (1996) filmed the wake of free swimming *Euchaeta rimana* using a Schlieren optical path. They found that both an adult female and a smaller copepodid shed vortices in their wake with the same frequency as that of the swimming leg oscillations. This is almost certainly also what happens in the wake of an escaping *T. longicornis*. Because the copepod is tethered in our study, the body of the animal does not move away from the vortex and the next oscillation of the swimming legs effectively 'feeds' the already existing vortex ring behind the animal. Only when the animal executes a few consecutive jumps, with a resting period of several tenths of a second inbetween, can we discern multiple vortices.

Energetics

T. longicornis moves its feeding appendages nearly 100% of the time. During feeding, the copepods in this study lost $1.1–3.0\times10^{-11}$ W due to viscous dissipation. Berner (1962) measured an average oxygen uptake of $0.0323\,\mu l\,O_2$ copepod^{-1} h^{-1} at 15°C. Taking an oxycaloric value of $1\,ml\,O_2$=20.1 J (Videler, 1993), this would amount to a total energy use of 1.8×10^{-7} W, indicating that the cost of the feeding current would be 0.0061–0.017% of the total energy budget. However, it would be unrealistic to assume that copepods can transfer metabolic energy into water movement without any losses along the way. Losses will occur because the mechanical efficiency of the motion of the moving limbs (η_p) and the efficiency with which muscles transfer chemical energy into kinetic energy (η_m) will both be less than 1. Total swimming efficiency (η_{tot}) can be calculated as:

$$\eta_{tot} = \eta_p \times \eta_m . \quad (6)$$

Using this model, Morris et al. (1985) calculated a value for η_p of 34% for the pereopod swimming of *Pleuromamma xiphias*, during escape swimming. Due to the jerky motion of

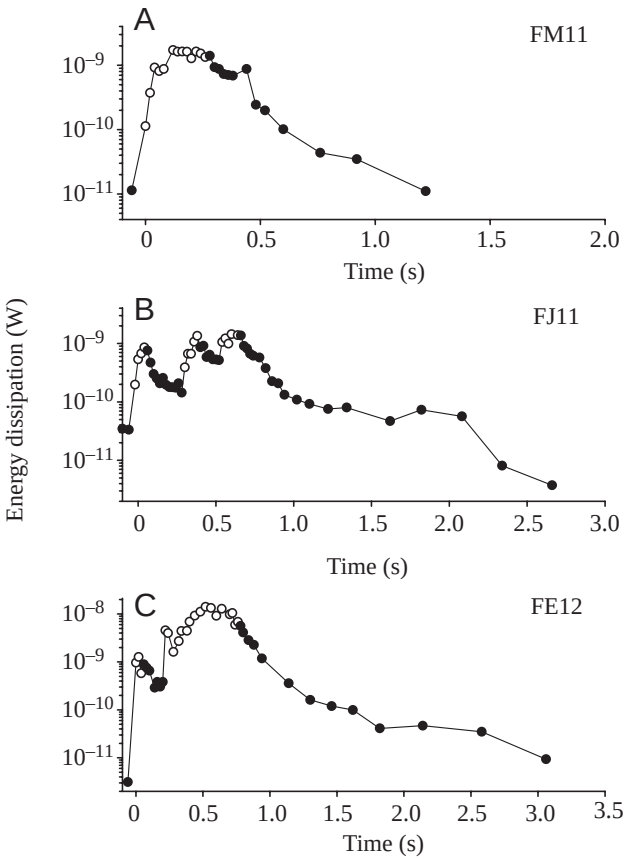

Fig. 10. (A–C). Rate of energy dissipation due to viscous friction in the wake of three escaping adult female *T. longicornis*. Open symbols indicate times when the swimming appendages were moving.

escape swimming, this is probably a rather high estimate for the mechanical efficiency of the smooth feeding current of *T. longicornis.* However, since no estimates for the mechanical efficiency of the mouth appendages is available, we will take this as a worst-case scenario. Assuming η_m to be 25% (Goldspink, 1977; Morris et al., 1985), the feeding current would still only account for 0.07–0.20% of the total energy budget.

Our study finds that the power delivered by the swimming legs during an escape response is 60–400 times higher than the mouth parts deliver while creating the feeding current. This is close to the figure mentioned by Strickler (1975, 1977), who argued that the energetic costs of high speed evasive movements would be 400-fold higher than the normal hop-and-sink swimming method of *Cyclops scutifer*. The behavioural experiments of van Duren and Videler (1996) indicated that, under their standard experimental conditions (presence of food, absence of kairomones or pheromones, no water movement), female *T. longicornis* escaped with a frequency of 0.3 jumps min^{-1} or 18 escape responses an hour. Assuming a mean leg movement duration of 0.2 s per escape response, this would result in a total mean swimming leg movement of 3.6 s per hour, or 0.1% of the animal's total time budget. Again, assuming the same values for η_p and η_m, this would translate into a total energy expenditure of between 2.3×10^{-11} and 1.1×10^{-10} W or 0.01–0.06% of the total energy budget. In the experiments of van Duren and Videler (1996) male *T. longicornis*, tested under the same circumstances, showed a fivefold higher escape frequency than the females. If females increased their escape frequency to this level, the increase of their energy consumption would be 0.07–0.3%. It appears therefore that only a very extreme increase in escape frequency may start to have a significant effect upon the energy budget of this species. This does not altogether mean that energy expenditure will never be an issue in copepod escape behaviour. Copepods often seem to fatigue after a number of escapes, e.g. after a number of successive attacks by a fish. The much higher energy demand of escape swimming could possibly lead to a short-term power transformation limitation even if the energy demand does not have an impact on the total budget.

Alcaraz and Strickler (1988) calculated that the routine hop and sink swimming of *C. scutifer*, performed with the swimming legs, accounted for 0.069% of its total energy budget. This is remarkably close to our estimates of the impact of the cost of the feeding current of *T. longicornis*, despite large differences in the way the two movements are created. Perhaps this relatively low cost of swimming can provide an explanation for the large variability of routine swimming and feeding movements among copepods. Optimising food intake is more important than minimising energy expenditure. Any extra cost involved in a change of swimming motion to facilitate food capture is not going to have a great impact on the total energy budget. Escape swimming, on the other hand, should by its very nature optimise the transfer of metabolic energy into forward motion. This may explain the fact that we find very little variation in escape kinematics among different copepod species.

We like to thank Per Jonsson and two anonymous referees for comments that helped to improve the manuscript. Eize Stamhuis is kindly acknowledged for valuable support during the implementation of his PIV technique.

References

Alcaraz, M., Paffenhöfer, G. A. and Strickler, J. R. (1980). Catching the algae: A first account of visual observations on filter feeding calanoids. In *Evolution and Ecology of Zooplankton Communities. Special symposium American Society of Limnology and Oceanography*, 57 edn. (ed. W. C. Kerfoot), pp. 241-248. Hanover: University Press of New England.

Alcaraz, M. and Strickler, J. R. (1988). Locomotion in copepods: pattern of movements and energetics of *Cyclops*. *Hydrobiologia* **167/168**, 409-414.

Andrews, J. C. (1983). Capture enhancement by deformation of the active space in the low reynolds number feeding current of calanoid copepods. *Can. J. Fish. Aq. Sci.* **40**, 1293-1302.

Barlow, D. I. and Sleigh, M. A. (1980). The propulsion and use of water currents for swimming and feeding in larval and adult A*rtemia*. In *The Brine Shrimp Artemia*, 12545 edn. (ed. G. Persoone, P. Sorgeloos, O. Roels and E. Jaspers), pp. 61-73. Wetteren: Universal Press.

Berner, A. (1962). Feeding and respiration in the copepod *Temora longicornis* (Müller). *J. Mar. Biol. Assn. UK* **42**, 625-640.

Buskey, E. J., Mann, C. G. and Swift, E. (1987). Photophobic responses

of calanoid copepods: possible adaptive value, *J. Plankton Res.* **9**, 857-870.

Emlet, R. B. (1990). Flow fields around ciliated larvae: effects of natural and artificial tethers. *Mar. Ecol. Prog. Ser.* **63**, 211-225.

Fields, D. and Yen, J. (1993). Outer limits and inner structure: The 3-dimensional flow field of *Pleuromamma xiphias* (Calanoida: Metrinidae). *Bull. Mar. Sci.* **53**, 84-95.

Gill, C. W. (1987). Recording the beat pattern of the second antennae of calanoid copepods. *Hydrobiologia* **148**, 73-78.

Goldspink, G. (1997). Muscle energetics and animal locomotion. In *Mechanics and Energetics of Animal Locomotion* (ed. R. M. Alexander and G. Goldspink), pp. 57-81. Chapman and Hall.

Granata, T. C. and Dickey, T. D. (1991). The fluid mechanics of copepods feeding in a turbulent flow: A theoretical approach. *Prog. Oceanog.* **26**, 243-261.

Hwang, J. S., Turner, J. T., Costello, J. H., Coughlin, D. J. and Strickler, J. R. (1993). A cinematographic comparison of behavior by the calanoid copepod *Centropages hamatus* Lilljeborg: Tethered versus free-swimming animals. *J. exp. mar. Biol. Ecol.* **167**, 277-288.

Hwang, J. S., Costello, J. H. and Strickler, J. R. (1994). Copepod grazing in turbulent flow: elevated foraging and habituation of escape responses. *J. Plankton Res.* **16**, 421-431.

Jiang, H., Meneveau, C. and Osborn, T. R. (1999). Numerical study of the feeding current around a copepod. *J. Plankton Res.* **21**, 1391-1421.

Jonsson, P. R. and Tiselius, P. (1990). Feeding behaviour, prey detection and capture efficiency of the copepod *Acartia tonsa* feeding on planktonic ciliates. *Mar. Ecol. Prog. Ser.* **60**, 35-44.

Klein Breteler, W. C. M. and Gonzales, S. R. (1986). Culture and development of *Temora longicornis* (Copepoda, Calanoida) at different conditions of temperature and food. *Syllogeus* **58**, 71-84.

Koehl, M. A. R. and Strickler, J. R. (1981). Copepods feeding current: Food capture at low Reynolds number. *Limnol. Oceanogr.* **26**, 1062-1073.

Légier-Visser, M. F., Mitchell, J. G., Okubo, A. and Fuhrman, J. A. (1986). Mechanoreception in calanoid copepods. A mechanism for prey detection. *Mar. Biol.* **90**, 529-535.

Morris, M. J., Kohlhage, K. and Gust, G. (1990). Mechanics and energetics of swimming in the small copepod *Acanthocyclops robustus* (Cyclopoida). *Mar. Biol.* **107**, 83-91.

Morris, M. J., Gust, G. and Torres, J. J. (1985). Propulsion efficiency and cost of transport for copepods: a hydromechanical model crustacean swimming. *Mar. Biol.* **86**, 283-295.

Pavlova, E. V. (1981). Rate of movements of copepods in plankton from the Indian ocean. *Ekologiya Morya* **5**, 61-65 [in Russian].

Saiz, E. and Kiørboe, T. (1995). Predatory and suspension feeding of the copepods *Acartia tonsa* in turbulent environments. *Mar. Ecol. Prog. Ser.* **122**, 147-158.

Singarajah, K. V. (1975). Escape reactions of zooplankton: effects of light and turbulence. *J. Mar. Biol. Assn. UK* **55**, 627-639.

Sleigh, M. A. and Barlow, D. I. (1980). Metachronism and control of locomotion in animals with many propulsive structures. In *Aspects of Animal Movement* (ed. H. Y. Elder and E. R. Trueman), pp. 49-67. Cambridge: Cambridge University Press.

Stamhuis, E. J. and Videler, J. J. (1995). Quantitative flow analysis around aquatic animals using laser sheet particle image velocimetry. *J. Exp. Biol.* **198**, 283-294.

Strickler, J. R. (1982). Calanoid copepods, feeding currents and the role of gravity. *Science* **218**, 158-160.

Strickler, J. R. (1977). Observation of swimming performances of planktonic copepods. *Limnol. Oceanogr.* **22**, 165-170.

Strickler, J. R. (1975). Swimming of planktonic Cyclops species (Copepoda, Crustacea): pattern, movements and their control. In *Swimming and Flying in Nature*, 12801 edn. (ed. T. Y. T. Wu, C. J. Brokaw and C. Brennen), pp. 599-614. New York: Plenum Press.

Tiselius, P. and Jonsson, P. R. (1990). Foraging behaviour of six calanoid copepods: observations and hydrodynamic analysis. *Mar. Ecol. Prog. Ser.* **66**, 23-33.

Trager, G., Achituv, Y. and Genin, A. (1994). Effect of prey escape ability, flow speed, and predator feeding mode on zooplankton capture by barnacles. *Mar. Biol.* **120**, 251-259.

van Duren, L. A., Stamhuis, E. J. and Videler, J. J. (1998). Reading the copepod personal ads: increasing encounter probability with hydromechanical signals. *Phil. Trans. R. Soc. Lond. B* **353**, 691-700.

van Duren, L. A., Stamhuis, E. J. and Videler, J. J. (2003). Copepod feeding currents: flow patterns, filtration rates and energetics. *J. Exp. Biol.* **206**, 255-267.

van Duren, L. A. and Videler, J. J. (1995). Swimming behaviour of developmental stages of the calanoid copepod *Temora longicornis* at different food concentrations. *Mar. Ecol. Prog. Ser.* **126**, 153-161.

van Duren, L. A. and Videler, J. J. (1996). The trade-off between feeding, mate seeking and predator avoidance in copepods: behavioural responses to chemical cues. *J. Plankton Res.* **18**, 805-818.

Videler, J. J. (1993). *Fish Swimming*. London: Chapman and Hall.

Vogel, S. (1981). *Life in Moving Fluids*. Boston: Willard Grant Press.

Yen, J. and Strickler, J. R. (1996). Advertisement and concealment in the plankton: what makes a copepod hydrodynamically conspicuous? *Invert. Biol.* **115**, 191-205.

Yen, J., Sanderson, B., Strickler, J. R. and Okubo, A. (1991). Feeding currents and energy dissipation by *Eucheta rimana*, a subtropical pelagic copepod. *Limnol. Oceanogr.* **36**, 362-369.